ACS Catalysis
Research Article
pubs.acs.org/acscatalysis

From Vanadia Nanoclusters to Ultrathin Films on TiO_2(110): Evolution of the Yield and Selectivity in the Ethanol Oxidation Reaction

Luca Artiglia,[†] Stefano Agnoli,[*,†] Letizia Savio,[‡] Jagriti Pal,[‡,§] Edvige Celasco,[‡,§] Mario Rocca,[‡,§] Federica Bondino,[∥] Elena Magnano,[∥] Carla Castellarin-Cudia,[⊥] Falko P. Netzer,[⊥] and Gaetano Granozzi[†]

[†]Department of Chemical Sciences, University of Padova, Via Marzolo 1, I-35131 Padova, Italy
[‡]IMEM CNR, UOS Genova, Via Dodecaneso 33, I-16146 Genova, Italy
[§]Department of Physics, University of Genova, Via Dodecaneso 33, I-16146 Genova, Italy
[∥]IOM CNR, LABORATORIO TASC, S.S. 14 Km. 163, 5, I-34149 Basovizza, TS, Italy
[⊥]Surface and Interface Physics, Institute of Physics, Karl-Franzens University Graz, A-8010 Graz, Austria

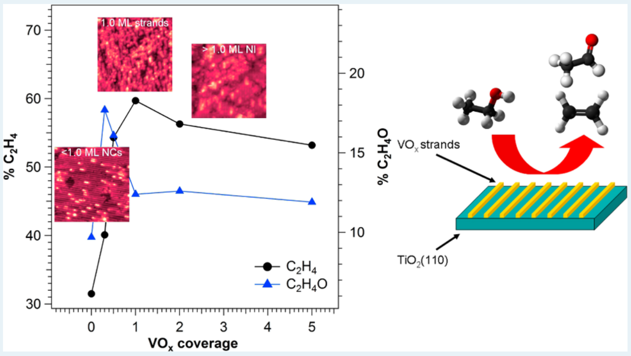

ABSTRACT: Oxide-on-oxide systems are becoming increasingly important in nanocatalysis and surface engineering, because of the creation of hybridized interfaces holding high reactivity and selectivity toward oxidation reactions. Here we report on the results of a multitechnique surface science study conducted on an oxide/oxide model system. By depositing increasing amounts of vanadium oxide (VO_x) on a titanium dioxide-rutile(110) substrate, we were able to follow the morphology and oxidation state of the overlayer. Three growth modes were detected: nanoclusters at low coverage (0.3 and 0.5 monolayer), one-dimensional strands aligned along the substrate [001] direction at monolayer coverage, and three-dimensional nanoislands at higher coverage (2.0 and 5.0 monolayers). All these structures share the same oxidation state (V_2O_3). We studied the reactivity and selectivity of these model catalysts toward partial oxidation of ethanol, finding that both of them depend on the VO_x thickness. Nanoclusters can yield acetaldehyde through low-temperature oxidative dehydrogenation but show a scarce selectivity in the investigated temperature range. The monolayer coverage is the most reactive toward ethanol dehydration to ethylene, showing also good selectivity. Similar results are found at high coverage, although the overall reactivity of the systems toward alcohol oxidation decreases.

KEYWORDS: *vanadium oxide, titanium dioxide, ethanol oxidation, nanocatalysis, oxidative dehydrogenation, dehydration*

■ INTRODUCTION

Nanocatalysis is today one of the most exciting subfields that has emerged from nanoscience. Some of its central interests are the control of chemical reactions by changing the size, dimensionality, chemical composition, and morphology of the catalysts and the quest for new catalytic systems obtained by the cooperative integration of different nano-objects. In particular, nanocatalysis studies have contributed to the change in the perspective on the standard view that assigns to metals the role of catalyst and to oxides the role of support, suggesting the idea that a careful design of the nanostructure of the materials can be even more effective than the intrinsic chemical nature as a tool for driving the reactivity toward specific byproducts.[1,2]

Supported vanadium oxide (VO_x) clusters and thin films have been widely studied because of their high activity in many relevant catalytic reactions. In particular, several studies were devoted to the vanadia/titania system either in the form of thin films supported on single crystals[3] or as large-surface area powders.[4] The TiO_2(110) surface was demonstrated to be a quite convenient substrate for the growth of vanadia layers with different structures and compositions, such as $VO_{x\cong 1}$,[5] disordered[6,7] and epitaxial V_2O_3,[8] stoichiometric pseudomorphic VO_2,[9] and V_2O_5,[10] providing a full gamut of model systems for a detailed investigation of the physicochemical properties of this system and paving the way for structure−activity studies. The most significant industrial application of VO_x is in the oxidation of SO_2 to SO_3 for the synthesis of H_2SO_4,[4] using a V_2O_5 alkali sulfate−pyrosulfate viscous melt on a SiO_2 substrate. Furthermore, V_2O_5 supported on various oxides is known to be an efficient catalyst for the oxidation of *o*-xylene to phthalic anhydride and for the selective catalytic reduction of NO_x emissions with ammonia or urea.[11,12] Recently, research efforts have focused on the study and development of highly

Received: June 24, 2014
Revised: September 2, 2014
Published: September 8, 2014

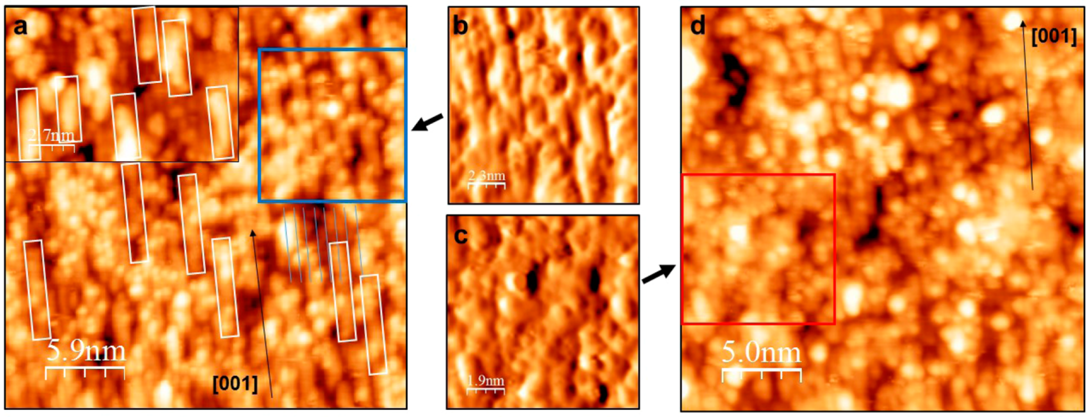

Figure 1. (a) STM image of the $TiO_2(110)$ (1 × 1) surface covered with 1.0 ML VO_x (290 Å × 290 Å, 2.1 V, 0.33 nA). The vanadia strands are outlined by white rectangles, and blue lines show the Ti 5-fold coordinated rows; the top left inset shows some vanadia strands nucleated on the Ti 5-fold coordinated rows. (b) Derivative image of the area outlined by the blue rectangle in panel a. (c) Derivative image of the area outlined by the red rectangle in panel d. (d) STM image of the $TiO_2(110)$ (1 × 1) surface covered with 5.0 ML VO_x (250 Å × 250 Å, 1.78 V, 0.70 nA).[38]

active catalysts for selective oxidation reactions: when supported on reducible oxides, VO_x promotes the oxidative dehydrogenation reactions (ODH) of short chain (C_2−C_4) alkanes to the corresponding alkenes, and of alcohols to the corresponding aldehydes.[4,13−16] The growing demand of olefins and aldehydes as fundamental raw materials for many industrial processes, e.g., the production of polyethylene, polypropylene, and resins, makes the study of ODH reactions of paramount importance.[4]

In the case of alcohols, the selectivity for aldehydes of the ODH process has a primary role in preventing their further oxidation to carboxylic acids. Both activity and selectivity of the catalysts strongly rely on the supporting material; e.g., reducible oxides (like TiO_2 or CeO_2) performed better than non-reducible ones (e.g., Al_2O_3 and SiO_2).[17−20] Moreover, VO_x coverage plays a key role, whereby submonolayer and monolayer species show the highest activity.[4,19,21]

Within this panorama, surface science (SS) can have an important impact in improving the understanding of the mechanisms at the basis of VO_x reactivity, as well as of the interplay between oxide nanophases and supports. Recent SS studies have demonstrated that a reducible support promotes ODH because it helps to stabilize the catalyst during the reaction steps.[22−30] It is known that the rate-determining step in the alcohol ODH reaction is the α-hydride elimination of adsorbed alkoxy groups. In this process, the alcohol is oxidized to the corresponding aldehyde, and at the same time, an electron is left on the VO_x catalyst. The reducibility of the support is essential for stabilizing this extra charge by means of charge transfer. This effect has been observed for VO_x/TiO_2,[23] VO_x/CeO_2,[27,30] (overlayer → support charge transfer) and CeO_x/TiO_2 (support → overlayer charge transfer).[22]

In this work, we have grown nanostructures of VO_x on TiO_2-rutile(110) in the 0.3−5.0 monolayer (ML) range, characterized them by SS tools, and studied their reactivity toward the ODH of ethanol (C_2H_5OH). Our first aim was to follow the structural and chemical evolution of the oxide/oxide model catalyst with increasing coverage by means of scanning tunneling microscopy (STM), X-ray photoelectron spectroscopy (XPS), X-ray absorption spectroscopy (XAS), and high-resolution electron energy loss spectroscopy (HREELS). Furthermore, we have studied the ethanol ODH reactivity of ethanol through temperature-programmed reaction (TPR) and HREELS, observing great changes in the total conversion yield and selectivity that corresponded to the different nanostructures.

The information provided by model studies can be used to improve our understanding of more complex real catalysts and of the single chemical steps involved in complex catalytic processes,[31] although it is essential to remember both the pressure and material gaps, which can limit the application of surface science findings.[32]

■ EXPERIMENTAL SECTION

The experiments were conducted in four different UHV systems placed in four different laboratories: Trieste, Genova, Padova, and Graz. The same $VO_x/TiO_2(110)$ preparation procedure[33,23] was reproduced in all the UHV systems: after several cycles of Ar^+ sputtering (1.0 keV), the TiO_2 rutile(110) substrate was flashed in UHV at 970 K, to get a sharp (1 × 1) surface reconstruction. Vanadium was deposited (from an electron beam evaporator) on the substrate held at 470 K, in a constant oxygen background ($p = 5 \times 10^{-8}$ mbar). The overlayer thickness was determined by angle-resolved XPS. The VO_x monolayer (ML) is defined as one V atom per $TiO_2(110)$-(1 × 1) surface unit cell and corresponds to 5.2×10^{14} V atoms/cm^2.

STM images were obtained at the Institute of Physics of the Karl-Franzens University Graz, using an Omicron micro-STM instrument operated at room temperature in constant current mode. Electrochemically etched W tips were employed, with typical sample biases between 1.2 and 3.0 V and tunneling currents between 0.3 and 1.5 nA.[7]

High-resolution XPS and XAS data were acquired in Trieste at the BACH beamline of the ELETTRA synchrotron light source. V 2p core level spectra were obtained with a photon energy of 597 eV and a pass energy (PE) of 20 eV, allowing a total resolution of 0.1 eV.

HREEL spectra were acquired at the Department of Physics of the University of Genoa in a multitechnique UHV chamber equipped with an HREEL spectrometer (Delta 0.5 by Specs). Energy loss spectra were acquired in specular geometry, with a primary electron energy E_e = 3.9 eV and an angle of incidence θ_i = 62°. A resolution between 5 and 8 meV was achieved in specular, depending on surface conditions. All curves are normalized to the elastic peak intensity.

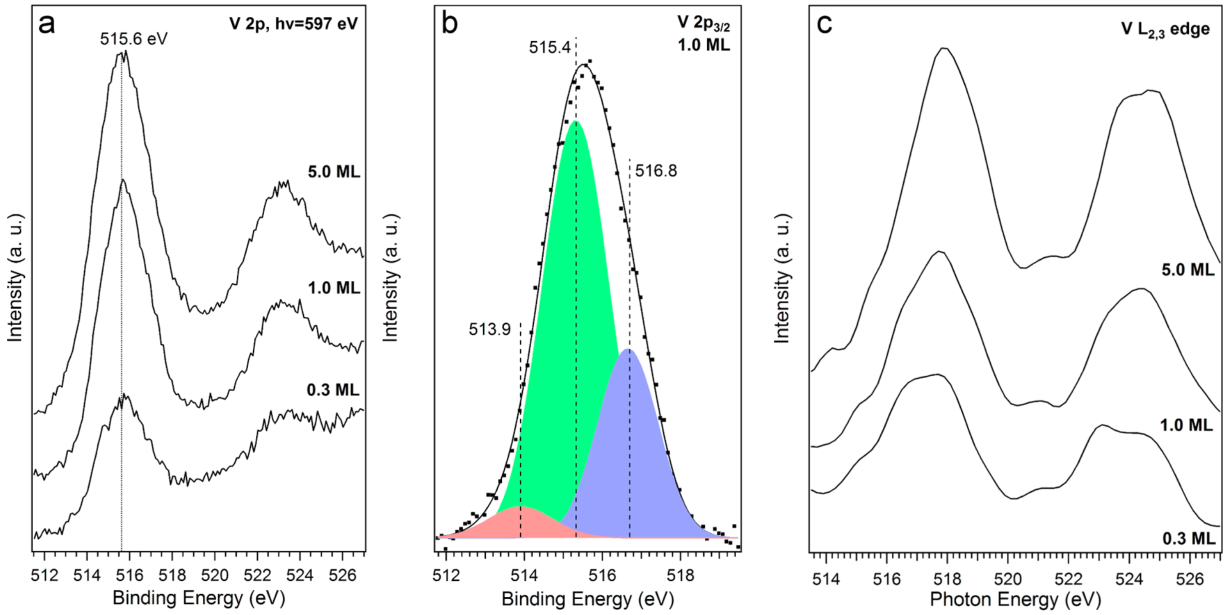

Figure 2. VO_x(0.3−5.0 ML)/TiO_2(110) thin films: (a) V 2p XPS spectra ($h\nu$ = 597 eV, normal emission, acquired at room temperature), (b) separation into single chemically shifted components of the V $2p_{3/2}$photoemission spectrum (1.0 ML VO_x coverage), and (c) XAS spectra of the V $L_{2,3}$ edge (normal emission).

TPR was performed at the Department of Chemical Sciences of the University of Padova in a multitechnique chamber equipped with a Hiden quadrupole mass spectrometer. The latter is provided with a quartz shield to minimize perturbations to the analysis of the desorption yield from the sample surface. The TiO_2(110) single crystal (10 mm × 5 mm, Mateck) was fixed to a Ta frame by means of a conductive ceramic glue and mounted on the manipulator head using two Ta wires (0.2 mm, Mateck). This sample holder allowed the exclusive analysis of the sample surface desorption products, as proven by preliminary C_2H_5OH desorption cycles, without contributions from the manipulator. After the sample had been cooled to 110 K, the desorption experiments were conducted with a heating rate of 2 K/s.

■ RESULTS AND DISCUSSION

Characterization of VO_x(0.3−5.0 ML)/TiO_2(110) Overlayers. A detailed STM study of the VO_x/TiO_2(110) model system (in the 0.15−5.0 ML VO_x range) was reported in 2004.[33] It was shown that, at low coverages (0.15−0.3 ML), oxide nanoclusters (NCs) nucleate and grow aligned along the substrate [001] direction. Such NCs have been recently characterized by STM, resonant photoemission spectroscopy (ResPes), and X-ray photoelectron diffraction (XPD), and their tetranuclear V_4O_6 structure has been demonstrated by comparison with density functional theory (DFT) calculations.[23]

Interestingly, these NCs share the same structure as the Ti_2O_3 strands that constitute the (1 × 2) reconstruction of rutile(110). Similar STM results were also previously obtained by Madix et al.,[34,35,7] who suggested the formation of V_2O_3 clusters isostructural to the Ti_2O_3 rows after the deposition of metal vanadium on differently reconstructed TiO_2(110) surfaces.

It is natural therefore that when the vanadia coverage is increased to 1 ML the NCs start to coalesce forming nanostructures ordered along the substrate [001] direction, hereafter called strands, as documented by the STM measurements reported in Figure 1a. The analysis of STM topographies indicates that the strands are nucleated on the rows constituted by 5-fold coordinated Ti ions (see the inset of Figure 1a and the derivative view in Figure 1b), the same nucleation sites as for the lower-coverage NCs.[33] The limited mobility of vanadium atoms on the TiO_2 surface, which is at the origin of the formation of tetrameric units at lower coverages, determines the rough growth morphology. As shown in Figure 1a, the strands are in general 4−8 nm long and occupy one substrate row. Moreover, before the completion of the first monolayer, some vanadia NCs are nucleated on the strands, increasing the level of corrugation of the surface. The formation of elongated oxide nanostructures on the TiO_2(110) surface appears to be a common phenomenon, because it has been observed also in the case of zirconium oxide and ruthenium oxide,[36,37] and it has always been connected to nanostructures with special chemical activity. In all these cases, structures very similar to the (1 × 2)-TiO_2 reconstruction were observed, even if the adsorbed oxides possess totally different bulk structures, as in the case of the Zr_2O_3 nanowires, where the +3 oxidation state of the metal is normally not stable in the bulk oxide.[37]

If the VO_x coverage is increased to 5.0 ML, the surface shows a clear morphological change (Figure 1d). Some strands are still present in the deeper layers, but most of the surface is covered by disordered randomly distributed three-dimensional nanoislands [hereafter called NI (see the derivative image in Figure 1c)], confirming previous works reporting a simultaneous multilayer or Frank-van der Merve growth mode.[6] The overall surface roughness is increased as well as the mean size of the islands with respect to the lower coverage. The reason for this morphological change can be traced back to the poor epitaxial match between the V_2O_3 and the TiO_2(110) surface. Actually, the V_2O_3 interfacial strands are stable only as monolayer phases and prevent the further growth of an epitaxial layer.

V 2p XPS spectra reported in Figure 2a for three VO_x coverages (0.3, 1.0, and 5.0 ML) show a broad $2p_{3/2}$ peak centered at ~515.6 eV that, in agreement with a previous investigation,[23] can be separated into three components (see Figure 2b): a minor peak at 513.9 eV, due to V^{2+} belonging to only partially oxidized NCs, and two main peaks at 515.4 and 516.8 eV, related to the multiplet structure of either V^{3+} or V^{4+} oxides.[39] It is extremely difficult to assign the V oxidation state on the basis of photoemission data, because V_2O_3 and VO_2 show similar multiplets.[39] On the other hand, XAS data (Figure 2c) can help us to distinguish between the various vanadium oxides based on their local structures. In particular, it is possible to find a good agreement between the literature data of V_2O_3 and the spectrum of the thickest VO_x film (5.0 ML), in terms of both prepeak and main absorption threshold positions and shape.[40] In their investigation of $VO_x/TiO_2(110)$, Madix et al. reported an XPS V $2p_{3/2}$ BE of 515.9 eV, similar to that observed in our experiments.[6,7] Moreover, the V $L_{2,3}$ absorption thresholds (Figure 2c) have the same features reported for both $VO_x/TiO_2(110)$ and $VO_x/\alpha\text{-}Al_2O_3(0001)$ and associated with V_2O_3, once again validating our assignment of stoichiometry.[6,7,41−43] Although our XAS data look similar (especially at 1.0 and 5.0 ML), it is possible to observe a trend passing from the lowest (i.e., NCs)[23] to the highest coverage. In fact, the shape of the multiplets in the V 2p spectra is related to the symmetry and spin of the ground state; thus, the absorption spectra reflect the differences among the local structure of V_4O_6 NCs (0.3 ML), strands (1.0 ML), and NI (2.0 and 5.0 ML). On the basis of the spectra reported in Figure 2, we can assume that NI have a V_2O_3 bulklike structure, while both strands and NCs, although having the same stoichiometry as NI, display a peculiar symmetry because of their strong hybridization with the TiO_2 substrate.

Low-energy electron diffraction (LEED) patterns (not shown), observed after each VO_x deposition, show that at low coverage (from 0.3 to 1.0 ML) the TiO_2 (1 × 1) surface reconstruction is still visible, although the spots become fuzzy. As already reported in previous studies,[9,30,31] in the 2.0−5.0 ML VO_x range the (1 × 1) LEED pattern is barely visible, suggesting that the substrate diffraction pattern is attenuated by a disordered overlayer.

In Figure 3a, we display the HREEL spectra (27−130 meV energy loss range) of the $TiO_2(110)$ substrate heated to 470 K in a 5.0×10^{-8} mbar oxygen background (same conditions used during the VO_x deposition), hereafter named "clean" TiO_2, and of five increasing VO_x coverages (0.3−5.0 ML range). The spectrum of the "clean" TiO_2 substrate shows the typical rutile(110) primary phonon losses, i.e., a double peak at 45 and 55 meV, and the Fuchs-Kliewer (FK) phonon at 94 meV.[44] The deposition of VO_x leads to two main effects already reported in the literature:[45] (i) the attenuation of the FK, due to the presence of an overlayer that quenches the TiO_2 lattice vibrational modes, and (ii) an overall shift of the double peak to lower energy losses and a change of its shape, due to the superposition with VO_x modes, whose intensity and, possibly, energy depend on coverage.[46] Comparing our results with the literature data, we were able to relate the double peak changes to the growth of VO_x primary phonon losses in the range of 40−90 meV.[47−49] Kresse et al. calculated by DFT the vibrational modes having a significant dipole intensity orthogonal to the surface plane for the different $V_2O_3(0001)$ surfaces and associated them with the experimental spectra.[47] It was found that the losses at <100 meV (47, 65, 78, and 92 meV) can be linked to the primary phonons of the V_2O_3 lattice.[47,48] A useful procedure for singling out VO_x-related losses is to calculate the HREELS difference spectra by subtracting the "clean" TiO_2 for each VO_x coverage. The results are shown in Figure 3b. Seven contributions can be singled out and are marked by lines. The 48, 64, and 79 meV peaks can be associated with the V_2O_3 lattice primary phonon losses, whereas the negative peaks at 55 and 94 meV are due to the attenuation of the substrate modes. The assignment of the 40 meV loss is not straightforward. A peak at such an energy was observed during the reduction of the highly oxidized VO_x monolayer structure ($\sqrt{7} \times \sqrt{7}$R19.1°) grown on Rh(111).[50] In this work, it has been proposed that the reduction of the pristine VO_x phase proceeds via the loss of V═O groups. In another paper, Langell et al. reported a 40 meV peak on MnO and assigned it to nonstoichiometric oxygen species.[51] Also, in the case presented here, the 40 meV peak might be ascribed to V−O vibrations of defects that are easily found on NCs, strands, and NI. Finally, with respect to the broad peak around 111 meV, whose intensity increases with a change from 0.5 to 5.0 ML VO_x, a similar energy loss was found on the $V_2O_3(0001)(\sqrt{3} \times \sqrt{3})$R30° O-rich surface, obtained by the oxidation of (1 × 1) vanadyl-terminated $V_2O_3(0001)$ films grown on Rh(111).[48] In the latter work, the authors singled out a phonon due to V═O at 129 meV, in good agreement with the results obtained for bulk V_2O_5.[52] Because there is no evidence of the formation of V═O groups on the present $VO_x/TiO_2(110)$ films, the 111 meV peak could be associated with V-reactive oxygen species ($V-O_r$) that are present on both VO_x strands and NI.

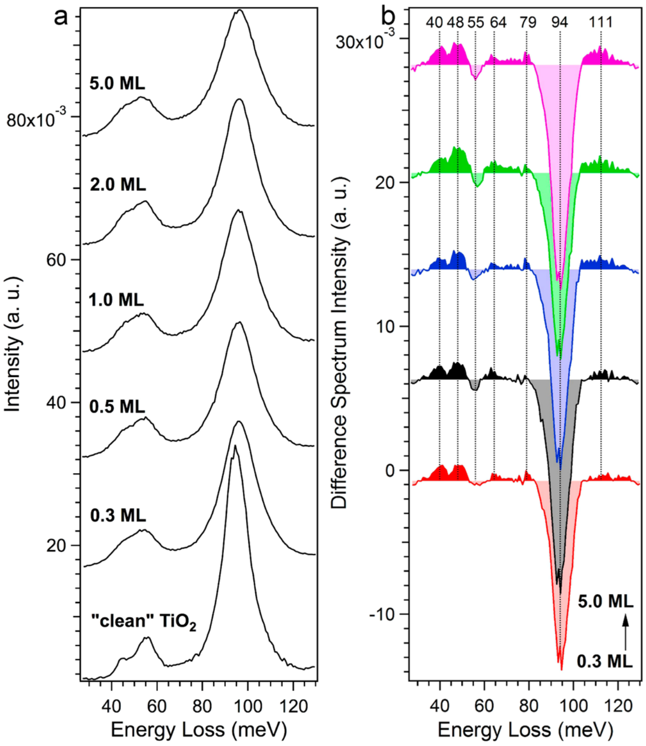

Figure 3. VO_x(0.3−5.0 ML)/$TiO_2(110)$ thin films: (a) HREELS data (recorded in specular) and (b) HREELS difference spectra calculated by subtracting the "clean" $TiO_2(110)$ spectrum (annealed under the same conditions that were used for VO_x growth) from each HREEL spectrum.

To summarize the structural data, we can hypothesize that, as long as the VO_x coverage is in the range of 0.3−1.0 ML, NCs with a formal V_2O_3 stoichiometry aggregate forming strands aligned with the TiO_2 crystal [001] direction. The reason for the stability of the V_2O_3 phase resides in the particular structure of the stripes, which is similar to that of the Ti_2O_3 chains[7,53−55] typical of the rutile(110) 1 × 2 reconstruction. The stabilization of vanadium species in an intermediate oxidation state may also be caused by the electronic hybridization at the interface, as already postulated for $CeO_x/TiO_2(110)$[22] and VO_x/CeO_2.[27]

Reactivity of $VO_x/TiO_2(110)$ with Ethanol. The reactivity of $VO_x/TiO_2(110)$ toward the oxidation of ethanol was tested by dosing the alcohol at low temperature and then heating the sample step by step following the surface reaction by TPR and HREELS.

In the case of the TPR spectra, 5 L of deuterium-labeled ethanol (C_2H_5OD) were dosed at 110 K. The use of isotopic labeling allowed easier analysis of the desorption products, and a better understanding of the overall reaction scheme. The *m/z* signals associated with different chemical species were acquired: C_2H_5OD, C_2H_5OH, carbon monoxide (CO), carbon dioxide (CO_2), water (H_2O and deuterated water, HDO and D_2O), acetaldehyde (C_2H_4O), ethylene (C_2H_4), acetic acid ($C_2H_4O_2$), and formaldehyde (CH_2O). Because of the overlap of *m/z* signals, a careful correction based on the ethanol cracking pattern was performed. The main desorption products are displayed in Figure 4: C_2H_5OD, C_2H_5OH, C_2H_4O, C_2H_4, D_2O, and H_2O. A CO_2 *m/z* signal, due to the complete oxidation of the alcohol, was detected as well but is not reported because of its low intensity. No other products were detected during the tests.

C_2H_5OD can be adsorbed on the surface either molecularly or dissociatively (reaction 1 or 2, respectively):

$$C_2H_5OD(g) \rightarrow C_2H_5OD(a) \tag{1}$$

$$C_2H_5OD(g) + O(s) \rightarrow C_2H_5O(a) + OD(a) \tag{2}$$

Its desorption can take place either molecularly (reaction 3) or recombinatively (reactions 4 and 5):

$$C_2H_5OD(a) \rightarrow C_2H_5OD(g) \tag{3}$$

$$C_2H_5O(a) + OD(a) \rightarrow C_2H_5OD(g) + O(s) \tag{4}$$

$$C_2H_5O(a) + OH(a) \rightarrow C_2H_5OH(g) + O(s) \tag{5}$$

Figure 4a reports the ethanol desorption profiles (all for the same exposure of 5 L) of the "clean" substrate and five VO_x coverages. In Table 1, we report the yield of carbon-containing species evaluated from the TPR data. For "clean" TiO_2, the C_2H_5OD and C_2H_5OH peaks have similar shapes and areas and reproduce well the data reported in the literature by Gamble et al. for the stoichiometric $TiO_2(110)$ surface.[56] The main peak, centered at ∼335 K, is due to molecular desorption, while the broad tail, extending to 450 K, is associated with recombinative desorption. Also, HREEL spectra (Figure 5) confirm that ethanol adsorption proceeds both molecularly and dissociatively. Figure 5a shows the HREEL spectra (120−490 meV energy range) of the different thin films before (1) and after (2) dosing 10 L of ethanol at 90 K and after thermalization at 200 K (3). The spectra of the surfaces before ethanol exposure are dominated by the TiO_2 substrate features: FK multiple peaks are found at 188, 282, and 376 meV, while the FK+double peak is found at 144 meV (peak centroid) and the FK+FK+double peak at 244 meV. After a 10 L C_2H_5OH dose, peaks at 130, 364, 406, and 460 meV can be detected (Figure 5b and Table 2). By comparison with the literature data, depending on the different substrates, values of $\nu(CCO)$ are reported between 114 and 133 meV values of $\nu(CH_3)$ between 357 and 370 meV and $\nu(OH)$ for molecularly adsorbed ethanol between 389 and 406 meV.[57,58] The 460 meV peak can be attributed to surface OH groups, formed in reaction 2, demonstrating that ethanol dissociative chemisorption takes place on the surfaces.[59]

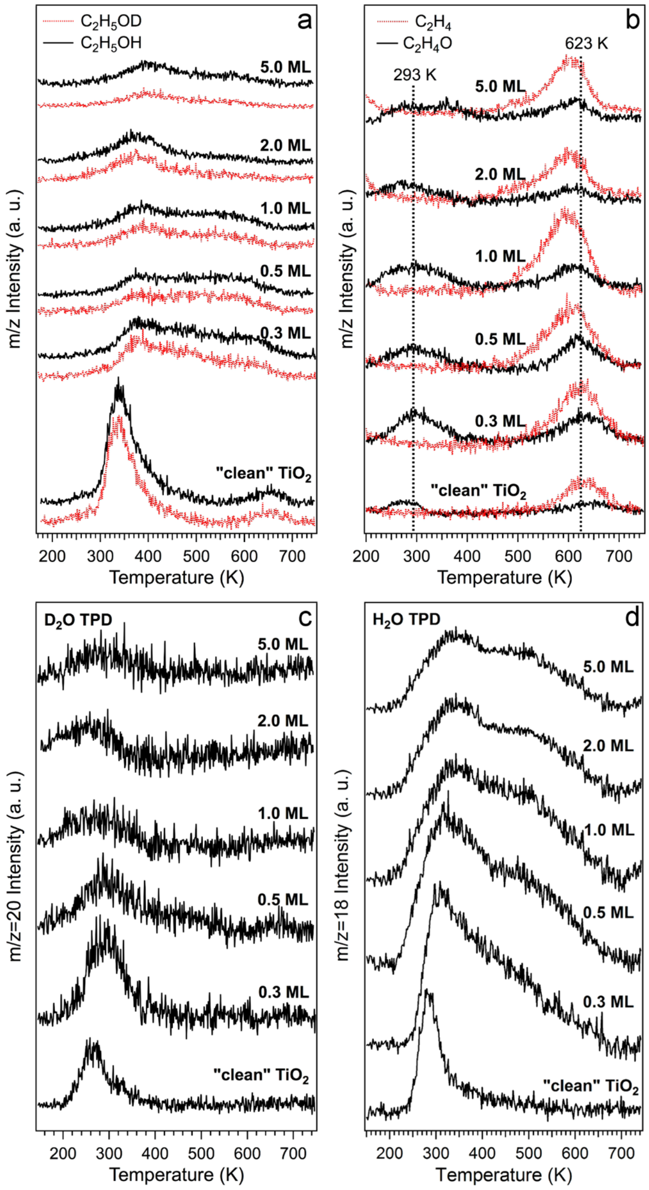

Figure 4. TPR spectra of VO_x(0.3−5.0 ML)/TiO_2(110) thin films recorded after a 5 L dosing of C_2H_5OD at 110 K: (a) C_2H_5OD and C_2H_5OH *m/z* signals, (b) acetaldehyde (C_2H_4O) and ethylene (C_2H_4) *m/z* signals, (c) deuterated water (D_2O) *m/z* signal, and (d) water (H_2O) *m/z* signal.

Ethanol TPR spectra (Figure 4a) of the "clean" substrate show that either the signal coming from deuterated or hydrogenated species displays a high-temperature peak at 650 K, a temperature close to that of C_2H_4 desorption, shown in Figure 4b (∼635 K). The ethanol dehydration reaction path, already reported for $TiO_2(110)$,[56,60] proceeds through the β-hydride elimination of adsorbed ethoxy groups:

$$C_2H_5O(a) \rightarrow C_2H_4(g) + OH(a) \tag{6}$$

Table 1. Yields of Carbon-Containing Species Evaluated from the TPR Data after Normalization to the Ethanol Cracking Pattern

	% ethanol (C_2H_5OH + C_2H_5OD)	% C_2H_4	% C_2H_4O (low temperature)	% C_2H_4O (high temperature)
"clean" TiO_2	52.0	31.5	6.8	9.7
0.3 ML VO_x	23.5	40.1	18.7	17.7
0.5 ML VO_x	15.7	54.3	13.9	16.1
1.0 ML VO_x	11.0	59.7	16.9	12.4
2.0 ML VO_x	14.6	56.3	16.5	12.6
5.0 ML VO_x	20.5	53.2	14.4	11.9

Table 2. HREELS Peak Assignments (Figure 5)

phonon (meV)	peak assignment
130	ν(CCO)
224	ν(CO), acetaldehyde
322	ν(CH), acetaldehyde
364	$\nu(CH_3)$
406	ν(OH), ethanol
424	ν(OH), H_2O
460	ν(OH), surface -OH groups

and leads to the formation of ethylene and surface hydroxyls, which can recombine with residual ethoxy groups to yield ethanol (reaction 5, high-temperature channel). Also, a small amount of C_2H_4O can be detected (see Figure 4b) as a broad peak centered around 293 K, whose formation is due to ODH reaction, originating from α-hydride elimination of adsorbed ethoxy groups:

$$C_2H_5O(a) + O(s) \rightarrow C_2H_4O(a) + OH(a) \qquad (7)$$

The same reaction was observed on stoichiometric $TiO_2(110)$,[56] and a peak related to the desorption of acetaldehyde was observed at 590 K on a {011}-faceted rutile-$TiO_2(001)$ surface.[60] In the analysis of ethanol desorption from $TiO_2(110)$, Farfan-Arribas and Madix[61] showed the simultaneous formation of ethylene and acetaldehyde (same relative amount) at 625 and 610 K, respectively. Moreover, they demonstrated that an increase in the substrate defect concentration (produced by ion sputtering) leads to an increase in the ethanol β-hydride elimination activity and to an overall negative shift of the desorption peak temperature (to ∼500 K).[61] The low-temperature activity toward ODH observed on our "clean" substrate could be related to the oxygen dosing at 470 K (as described above), which can promote the formation of TiO_x reconstructions holding reactive oxygen species.[62]

Interestingly, ethanol amounts to 50% of all desorption species on the "clean" substrate, whereas the VO_x films are more chemically active; only a quantity ranging from 11 to 23.5% of the desorption products is represented by ethanol (see Table 1). On the "clean" TiO_2 surface, ethanol desorbs at 335 K, to be compared with a temperature of 375 K on the vanadia-covered surfaces; moreover, the peak is broader in the latter case, showing a shoulder extending to 660 K. This is indicative of two reaction channels (see Figure 4b), i.e., low- and high-temperature recombinative desorption. It is noteworthy that, as long as the VO_x coverage is increased, the shoulder in the main peak shifts to a lower temperature.

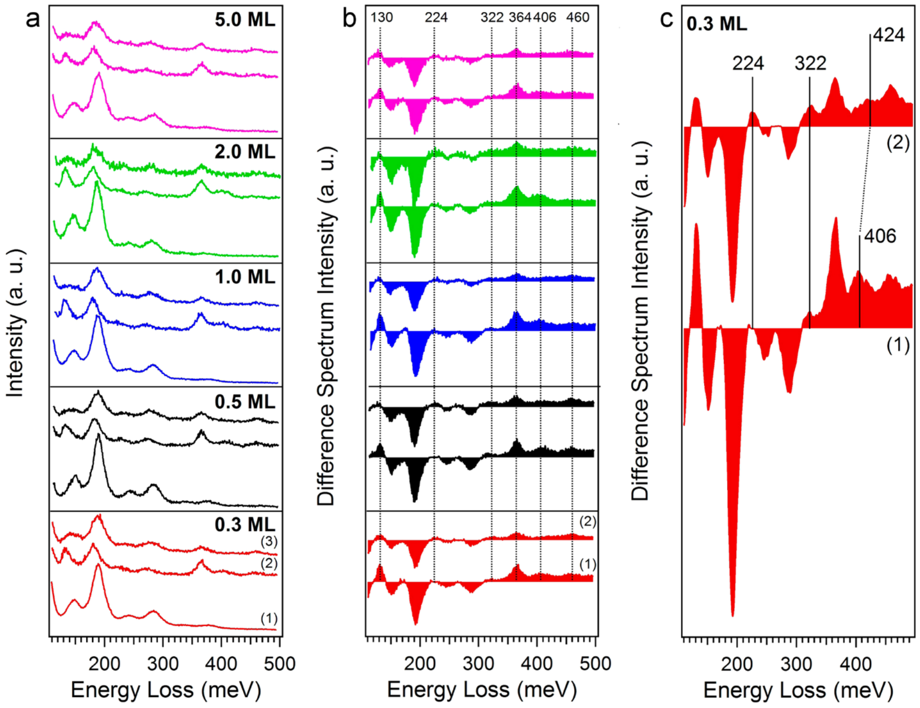

Figure 5. (a) HREEL spectra of VO_x(0.3–5.0 ML)/$TiO_2(110)$ thin films: (1) "clean" surface at 90 K, (2) after a 10 L C_2H_5OH dosing, and (3) after thermalization at 200 K. (b) HREELS difference spectra calculated by subtracting the spectra of the "clean" $VO_x/TiO_2(110)$ surface from the corresponding spectra acquired (1) after a 10 L C_2H_5OH dosing and (2) after thermalization at 200 K. (c) Magnification of the HREELS difference spectra for the VO_x(0.3 ML)/$TiO_2(110)$ surface.

Moreover, in the case of the C_2H_5OD signal, the intensity coming from the high-temperature desorption channel decreases with a change from 0.3 to 5.0 ML VO_x.

With regard to the C_2H_4 desorption spectra (Figure 4b), a peak centered at ~623 K is observed for the VO_x(0.3 ML)/TiO_2 surface. It moves to a lower temperature as a function of VO_x coverage, reaching 595 K at 1.0 ML, and then shifts back to 605 K for both 2.0 and 5.0 ML. As already observed for the "clean" TiO_2, there is a clear correlation between the C_2H_4 and the high-temperature C_2H_5OH desorption peak, related to β-hydride elimination (reaction 6), that eventually leads to the formation of surface -OH, which recombine with the ethoxy species to yield C_2H_5OH. From the comparison of the C_2H_4 TPR spectra (Figure 4b), we can obtain the following information. (i) VO_x is a promoter for β-hydride elimination. A clear peak shift (from 645 to 623 K) is observed after comparison of the "clean" $TiO_2(110)$ substrate with VO_x(0.3 ML)/$TiO_2(110)$, together with a 9% increase in the yield of C_2H_4 (see Table 1). (ii) Reaction 6 is favored on VO_x strands, as demonstrated by the lower C_2H_4 desorption temperature, which means a lower activation energy, together with the highest product yield [~60% (see Table 1)]. The overall yield of C_2H_4 (Table 1) exhibits a volcano curve behavior with respect to VO_x coverage, where a coverage of 1.0 ML is the most active toward the ethanol dehydration reaction and strongly favors the partial oxidation of ethanol, as demonstrated by the lowest yield of C_2H_5OH and C_2H_5OD (11%).

We can correlate this to the presence of linear nanostructures with a formal V_2O_3 stoichiometry, previously described as strands, which grow aligned along the [001] direction, filling the channels defined by the bridging oxygen rows, and experience a special interfacial hybridization with the substrate,[23] which is responsible for a facilitated charge transfer from vanadia to the TiO_2 substrate, and therefore the reduced cost of oxygen vacancy formation.

Interestingly, experimental evidence of active surface oxygen species connected to vanadia is provided by HREELS. Even if this is not a quantitative technique, it indicates that the signal at 111 meV, associated with V$-O_r$, correlates well with the trend in the yield of C_2H_4, suggesting that these species can be responsible for the β-hydride elimination reaction.

The other main reaction product of ethanol decomposition is C_2H_4O, which is formed through α-hydride elimination of adsorbed ethoxy groups (reaction 7) and shows peaks at both low (~293 K) and high (~630 K) desorption temperatures. Several important outcomes can be deduced from the TPR experiments reported in Figure 4b. (i) The presence of VO_x promotes the ethanol ODH reaction such as in the case of C_2H_4. The overall C_2H_4O yield increases from 16% ("clean" TiO_2) to 36% (after the deposition of 0.3 ML VO_x) and then decreases monotonically with VO_x coverage. (ii) The catalyst selectivity is affected by the amount of deposited VO_x: at low coverages (0.3 and 0.5 ML), C_2H_4O is formed efficiently at both temperatures (see Table 1), whereas at high coverages (1.0, 2.0, and 5.0 ML), the C_2H_4O desorption features are quenched. The overall C_2H_4O yield gradually decreases from 36% at 0.3 ML to 26% at 5.0 ML (see Table 1). (iii) As observed before for C_2H_4, the high-temperature desorption peaks undergo a negative temperature shift as a function of VO_x coverage (from 620 K at 0.3 ML to 595 K at 1.0 ML and then to 600 at 2.0 and 5.0 ML). Once again, the VO_x strands are shown to be the most active in the high-temperature channel. (iv) At low temperatures, the C_2H_4O yield is scarcely coverage-dependent. The deposition of VO_x causes a small shift of this peak (~10 K) with respect to the "clean" TiO_2 substrate. Because this peak does not change substantially with coverage, we can consider the reactivity toward the low-temperature C_2H_5OH ODH reaction intrinsic to VO_x.

The formation of C_2H_4O was reported also on bulk V_2O_5,V_2O_5/CeO_2, V_2O_5/TiO_2, and V_2O_5/SiO_2 surfaces at temperatures ranging from 450 to 610 K, depending both on the vanadia load and on the type of support (CeO_2 and TiO_2 were the most active).[25,63] These papers assert that the monolayer V_2O_5 is the most active catalyst and its deactivation is due both to the agglomeration of NCs into crystallites (favored on nonreducible oxides like SiO_2)[63] and the reduction of vanadium ions. The role of the support is discussed in a work by Beck et al.,[31] reporting ethanol TPR measurements of VO_x NCs (dimeric, trimeric, and larger oligomeric species), deposited on either Al_2O_3 or CeO_2. The results show that the VO_x/Al_2O_3 system is not reactive, while in the case of VO_x/CeO_2, C_2H_4O desorbs at 500 and 600 K, where the former peak is attributed to ODH catalyzed by VO_x species.[31] These experimental results are supported by DFT calculations indicating that on the VO_x/CeO_2 system the oxygen defect formation energy is ~5 times lower than on VO_x/Al_2O_3. More recently, the VO_x(NCs)/$CeO_2(111)$ model system has been thoroughly investigated (DFT) by Penschke et al., demonstrating that vanadyl-terminated monomers (VO_2) are the most active species, with the lowest oxygen defect formation energy and undergoing exothermic hydrogenation.[30]

Our results are in good agreement with these findings; i.e., the VO_x/TiO_2 interface activates a low-temperature dehydrogenation path, yielding C_2H_4O at an unprecedented low temperature (~300 K). Similar results were reported recently for methanol ODH on VO_x(0.3 ML)/$TiO_2(110)$ and attributed both to the peculiar structure of the NCs and to the interplay between the NCs and the substrate in terms of stabilization due to NC → TiO_2 extra-charge transfer during the reaction and the associated reduced cost for oxygen vacancy formation.[23] In fact, the evaluation of the yield of carbon-containing species reported in Table 1 demonstrates that the VO_x NCs are the most effective catalysts with respect to the low-temperature ODH reaction (18.7% yield).

The D_2O (Figure 4c) and H_2O (Figure 4d) TPR data complete the description of the reactivity scenario. Water is formed by recombinative desorption of hydroxyl groups (hydroxyls are formed by reactions 6 and 7) according to reactions 8−10:

$$OD(a) + OD(a) \rightarrow D_2O(g) + O(s) \tag{8}$$

$$OH(a) + OD(a) \rightarrow HDO(g) + O(s) \tag{9}$$

$$OH(a) + OH(a) \rightarrow H_2O(g) + O(s) \tag{10}$$

In the case of D_2O, a single peak, centered at ~290 K, is found at 0.3 ML VO_x. It decreases and broadens as a function of coverage, following the trend of the C_2H_4O low-temperature desorption peak (Figure 4b). The H_2O m/z signal shows two clear desorption features, centered at ~305 and ~500 K. The relative intensity of the 500 K peak increases with the change from 0.3 to 1.0 ML VO_x and then decreases again at 2.0 and 5.0 ML VO_x. HDO desorption spectra (not reported) resemble those of H_2O. Because -OH groups are formed as a consequence of both α- and β-hydride elimination of the adsorbed ethoxy intermediates (reactions 6 and 7, respectively),

H_2O desorption peaks can trace the temperature evolution of these reactions. A first process occurs between 290 and 300 K, which is due to α-hydride elimination because only C_2H_4O desorption peaks are found in this range. On the other hand, the 500 K desorption can be due to either α- or β-hydride elimination, as both C_2H_4 and C_2H_4O are desorbed between 590 and 645 K.

The body of our TPR spectra indicates that when the VO_x NCs are the prevalent surface species, the catalyst is very active toward low-temperature ODH. Ethanol is dissociated (reaction 2) both on the NCs and on the TiO_2 substrate, and -OD groups recombine to form D_2O at 290 K (reaction 8), leaving surface oxygen species available for the α-hydride elimination of adsorbed ethoxy groups (reaction 7).[23] At higher VO_x coverages (from 1.0 to 5.0 ML, where VO_x strands and NI are present), the level of D_2O formation is lower, and this reflects the overall C_2H_4O yield. This could be due to a competition between reaction 7 (ODH) and reaction 4 (recombinative desorption) and could mean that, on VO_x strands and NI, there is less proximity between OD groups. This hypothesis is supported by the data for H_2O desorption (Figure 4d): the low-temperature peak (~305 K), whose intensity is higher at 0.3 ML, is due to reaction 10, taking place between -OH groups formed after α-hydride elimination (although we cannot exclude the presence of surface -OH groups due to some small amount of water contamination). Further proof of this reaction mechanism is that the C_2H_4O and H_2O low-temperature desorption peaks occur in the same temperature range (around 300 K).

The H_2O high-temperature desorption peak develops between 400 and 620 K and reaches its maximal intensity at 1.0 ML. The highest C_2H_4 yield is found at this coverage, as well, meaning that such desorption peaks are mainly related to β-hydride elimination.

Surprisingly, the desorption of C_2H_4 from the surface takes place only after water desorption (peak maxima between 590 and 645 K), suggesting a strong interaction between the vanadia layer and the ethylene precursor. Our desorption data, however, are in agreement with the results of Lee et al.,[64] who reported that ethylene desorbs in the temperature range of 500−700 K from a strongly reduced (V^{2+}/V^{3+}) vanadia surface. On the other hand, the presence of reduced sites is very likely considering the overall reducing effect of ethanol on the vanadia surface.

The HREELS (Figure 5) data are in good agreement with the special reactivity toward low-temperature ethanol ODH shown by TPR. The difference spectra displayed in Figure 5c for the 0.3 ML VO_x sample demonstrate that a thermal treatment at 200 K, which promotes the removal of a physisorbed ethanol multilayer, quenches the 130, 364, and 406 meV phonons, while a new peak appears at 424 meV. This new peak can be associated with H_2O, formed during reactions 8−10.[59] Moreover, new peaks are found at 224 and 322 meV (see Figure 5b,c). The former can be associated with ν(CO), although blue-shifted with respect to the values reported in the literature about C_2H_4O adsorption on various substrates (between 206 and 217 meV).[65−68] The peak at 322 meV is compatible with the ν(CH) values of adsorbed acetaldehyde, although it is red-shifted with respect to the reported values (between 340 and 350 meV).[65,66]

CONCLUSION

The growth of VO_x overlayers on TiO_2-rutile(110) has been studied by STM, XPS, XAS, and HREELS. Different nanostructures sharing the same oxidation state were observed, depending on the VO_x coverage. At low coverage, NCs grown on top of the 5-fold coordinated Ti ion rows of the TiO_2 substrate in the [001] direction were found, in agreement with previous results.[7] Once the coverage was increased to 1 ML, strandlike nanostructures aligned along the [001] direction were detected. A further increase (to 2.0 and 5.0 ML) led to V_2O_3 NI growing randomly on the substrate.

A combined TPR and HREELS analysis of the reactivity of $VO_x/TiO_2(110)$ model catalysts toward the oxidation of ethanol revealed that partial oxidation is strongly favored on all substrates (almost no CO or CO_2, because of the complete oxidation reaction path, observed) even though significant differences in the selectivity, depending on the VO_x loading, were detected. This intrinsic high selectivity can be connected to the relatively low oxidation state of vanadia (V^{3+}), stabilized by the interaction with the substrate that prevents a more advanced oxidation such as in the case of V_2O_5.[16,46]

Two reaction channels, i.e., a low-temperature one (from 200 to 400 K) and a high-temperature one (from 450 to 700 K), are present for all the analyzed systems.

At low coverage (0.3 and 0.5 ML), the ODH reaction yielding acetaldehyde was observed at an unprecedented low temperature (~300 K), although the catalysts demonstrated poor selectivity. The vanadia monolayer showed a peculiar catalytic behavior, with the highest ethanol conversion and selectivity toward the formation of ethylene occurring at ~590 K. Both the low-temperature ODH shown by the NCs and the high selectivity toward ethanol dehydration of the VO_x ML can be traced back to the presence of nanostructures (NCs and strands) that are strongly hybridized with the TiO_2 substrate.[23] In fact, the ODH of ethanol requires a strong stabilization of the activated complexes during the reaction, and this can be achieved efficiently when extra charges are transferred from the overlayer to the substrate, stabilizing the reduced form of the catalyst.[23] Further evidence of the special chemical activity associated with the oxide/oxide interface comes from the analysis of the reactivity at the highest coverages (2.0 and 5.0 ML): the ethanol conversion and the selectivity toward low-temperature ODH progressively decrease (see Table 1).

Our work therefore helps to substantiate an emerging paradigm in nanocatalysis,[27,23,22,69] which exploits the possibility of an easy electron banking at the interface as a way to lower the activation barrier of redox reactions.

In conclusion, this work provides an interpretation of the structure−reactivity interplay in VO_x/TiO_2-rutile(110) model catalysts. Because nanocatalysis surface science studies are very useful in revealing the mechanisms of real catalytic reactions, the results obtained can be exploited for the controlled synthesis of new materials with high reactivity and selectivity.

AUTHOR INFORMATION

Corresponding Author

*E-mail: stefano.agnoli@unipd.it.

Notes

The authors declare no competing financial interest.

■ ACKNOWLEDGMENTS

This work has been funded by the Italian Ministry of Instruction, University and Research (MIUR) through FIRB Project RBAP115AYN ("Oxides at the nanoscale: multifunctionality and applications") and by Compagnia San Paolo. J.P. acknowledges financial support through a postdoctoral grant from the ICTP-Tril program.

■ REFERENCES

(1) Kuhlenbeck, H.; Shaikhutdinov, S.; Freund, H. J. *Chem. Rev.* **2013**, *113*, 3986−4034.

(2) Romanyshyn, Y.; Guimond, S.; Kuhlenbeck, H.; Kaya, S.; Blum, R. P.; Niehus, H.; Shaikhutdinov, S.; Simic-Milosevic, V.; Nilius, N.; Freund, H. J.; Ganduglia-Pirovano, M. V.; Fortrie, R.; Dobler, J.; Sauer, J. *Top. Catal.* **2008**, *50*, 106−115.

(3) Surnev, S.; Ramsey, M. G.; Netzer, F. P. *Prog. Surf. Sci.* **2003**, *73*, 117−165.

(4) Wachs, I. E. *Dalton Trans.* **2013**, *42*, 11762−11769.

(5) Della Negra, M.; Sambi, M.; Granozzi, G. *Surf. Sci.* **2000**, *461*, 118−128.

(6) Biener, J.; Baumer, M.; Madix, R. J. *Surf. Sci.* **1999**, *432*, 178−188.

(7) Madix, R. J.; Biener, J.; Baumer, M.; Dinger, A. *Faraday Discuss.* **1999**, *114*, 67−84.

(8) Sambi, M.; Della Negra, M.; Granozzi, G. *Surf. Sci.* **2000**, *470*, L116−L122.

(9) Sambi, M.; Della Negra, M.; Granozzi, G. *Thin Solid Films* **2001**, *400*, 26−36.

(10) Wang, Q. G.; Madix, R. J. *Surf. Sci.* **2001**, *474*, L213−L216.

(11) Wachs, I. E.; Weckhuysen, B. M. *Appl. Catal., A* **1997**, *157*, 67−90.

(12) Centi, G. *Appl. Catal., A* **1996**, *147*, 267−298.

(13) Blasco, T.; Nieto, J. M. L. *Appl. Catal., A* **1997**, *157*, 117−142.

(14) Cavani, F.; Ballarini, N.; Cericola, A. *Catal. Today* **2007**, *127*, 113−131.

(15) Deo, G.; Wachs, I. E. *J. Catal.* **1994**, *146*, 323−334.

(16) Weckhuysen, B. M.; Keller, D. E. *Catal. Today* **2003**, *78*, 25−46.

(17) Daniell, W.; Ponchel, A.; Kuba, S.; Anderle, F.; Weingand, T.; Gregory, D. H.; Knozinger, H. *Top. Catal.* **2002**, *20*, 65−74.

(18) Dinse, A.; Frank, B.; Hess, C.; Habel, D.; Schomacker, R. *J. Mol. Catal. A: Chem.* **2008**, *289*, 28−37.

(19) Wachs, I. E. *Catal. Today* **2005**, *100*, 79−94.

(20) Baldychev, I.; Vohs, J. M.; Gorte, R. J. *Appl. Catal., A* **2011**, *391*, 86−91.

(21) Wang, Q. G.; Madix, R. J. *Surf. Sci.* **2002**, *496*, 51−63.

(22) Agnoli, S.; Reeder, A. E.; Senanayake, S. D.; Hrbek, J.; Rodriguez, J. A. *Nanoscale* **2014**, *6*, 800−810.

(23) Artiglia, L.; Agnoli, S.; Vittadini, A.; Verdini, A.; Cossaro, A.; Floreano, L.; Granozzi, G. *J. Am. Chem. Soc.* **2013**, *135*, 17331−17338.

(24) Feng, T.; Vohs, J. M. *J. Catal.* **2004**, *221*, 619−629.

(25) Feng, T.; Vohs, J. M. *J. Phys. Chem. B* **2004**, *108*, 5647−5652.

(26) Feng, Z. X.; Lu, J. L.; Feng, H.; Stair, P. C.; Elam, J. W.; Bedzyk, M. J. *J. Phys. Chem. Lett.* **2013**, *4*, 285−291.

(27) Ganduglia-Pirovano, M. V.; Popa, C.; Sauer, J.; Abbott, H.; Uhl, A.; Baron, M.; Stacchiola, D.; Bondarchuk, O.; Shaikhutdinov, S.; Freund, H. J. *J. Am. Chem. Soc.* **2010**, *132*, 2345−2349.

(28) Goebke, D.; Romanyshyn, Y.; Guimond, S.; Sturm, J. M.; Kuhlenbeck, H.; Dobler, J.; Reinhardt, U.; Ganduglia-Pirovano, M. V.; Sauer, J.; Freund, H. J. *Angew. Chem., Int. Ed.* **2009**, *48*, 3695−3698.

(29) Gonzalez-Navarrete, P.; Gracia, L.; Calatayud, M.; Andres, J. *J. Phys. Chem. C* **2010**, *114*, 6039−6046.

(30) Penschke, C.; Paier, J.; Sauer, J. *J. Phys. Chem. C* **2013**, *117*, 5274−5285.

(31) Beck, B.; Harth, M.; Hamilton, N. G.; Carrero, C.; Uhlrich, J. J.; Trunschke, A.; Shaikhutdinov, S.; Schubert, H.; Freund, H. J.; Schlogl, R.; Sauer, J.; Schomacker, R. *J. Catal.* **2012**, *296*, 120−131.

(32) Goodman, D. W. *Chem. Rev.* **1995**, *95*, 523−536.

(33) Agnoli, S.; Sambi, M.; Granozzi, G.; Castellarin-Cudia, C.; Surnev, S.; Ramsey, M. G.; Netzer, F. P. *Surf. Sci.* **2004**, *562*, 150−156.

(34) Biener, J.; Wang, J.; Madix, R. J. *Surf. Sci.* **1999**, *442*, 47−54.

(35) Biener, J.; Baumer, M.; Wang, J.; Madix, R. J. *Surf. Sci.* **2000**, *450*, 12−26.

(36) Yang, F.; Kundu, S.; Vidal, A. B.; Graciani, J.; Ramirez, P. J.; Senanayake, S. D.; Stacchiola, D.; Evans, J.; Liu, P.; Sanz, J. F.; Rodriguez, J. A. *Angew. Chem., Int. Ed.* **2011**, *50*, 10198−10202.

(37) Reeder, A. E.; Agnoli, S.; Rizzi, G. A.; Granozzi, G. *J. Phys. Chem. C* **2014**, *118*, 8026−8033.

(38) Horcas, I.; Fernandez, R.; Gomez-Rodriguez, J. M.; Colchero, J.; Gomez-Herrero, J.; Baro, A. M. *Rev. Sci. Instrum.* **2007**, *78*, 013705.

(39) Demeter, M.; Neumann, M.; Reichelt, W. *Surf. Sci.* **2000**, *454*, 41−44.

(40) Abbate, M.; Pen, H.; Czyzyk, M. T.; Degroot, F. M. F.; Fuggle, J. C.; Ma, Y. J.; Chen, C. T.; Sette, F.; Fujimori, A.; Ueda, Y.; Kosuge, K. *J. Electron Spectrosc. Relat. Phenom.* **1993**, *62*, 185−195.

(41) Price, N. J.; Reitz, J. B.; Madix, R. J.; Solomon, E. I. *J. Electron Spectrosc. Relat. Phenom.* **1999**, *98*, 257−266.

(42) Biener, J.; Baumer, M.; Madix, R. J.; Liu, P.; Nelson, E. J.; Kendelewicz, T.; Brown, G. E. *Surf. Sci.* **1999**, *441*, 1−9.

(43) Baumer, M.; Biener, J.; Madix, R. J. *Surf. Sci.* **1999**, *432*, 189−198.

(44) Cox, P. A.; Egdell, R. G.; Eriksen, S.; Flavell, W. R. *J. Electron Spectrosc. Relat. Phenom.* **1986**, *39*, 117−126.

(45) Guo, Q.; Lee, S.; Goodman, D. W. *Surf. Sci.* **1999**, *437*, 38−48.

(46) Savio, L.; Celasco, E.; Vattuone, L.; Rocca, M.; Senet, P. *Phys. Rev. B* **2003**, *67*, 075420.

(47) Kresse, G.; Surnev, S.; Schoiswohl, J.; Netzer, F. P. *Surf. Sci.* **2004**, *555*, 118−134.

(48) Pfuner, F.; Schoiswohl, J.; Sock, M.; Surnev, S.; Ramsey, M. G.; Netzer, F. P. *J. Phys.: Condens. Matter* **2005**, *17*, 4035−4047.

(49) Surnev, S.; Kresse, G.; Sock, M.; Ramsey, M. G.; Netzer, F. P. *Surf. Sci.* **2001**, *495*, 91−106.

(50) Schoiswohl, J.; Surnev, S.; Sock, M.; Eck, S.; Ramsey, M. G.; Netzer, F. P.; Kresse, G. *Phys. Rev. B* **2005**, *71*, 165437.

(51) Langell, M. A.; Hutchings, C. W.; Carson, G. A.; Nassir, M. H. *J. Vac. Sci. Technol., A* **1996**, *14*, 1656−1661.

(52) Poelman, H.; Vennik, J.; Dalmai, G. *J. Electron Spectrosc.* **1987**, *44*, 251−262.

(53) Ng, K. O.; Vanderbilt, D. *Phys. Rev. B* **1997**, *56*, 10544−10548.

(54) Onishi, H.; Fukui, K.; Iwasawa, Y. *Bull. Chem. Soc. Jpn.* **1995**, *68*, 2447−2458.

(55) Blanco-Rey, M.; Abad, J.; Rogero, C.; Mendez, J.; Lopez, M. F.; Martin-Gago, J. A.; de Andres, P. L. *Phys. Rev. Lett.* **2006**, *96*, 055502.

(56) Gamble, L.; Jung, L. S.; Campbell, C. T. *Surf. Sci.* **1996**, *348*, 1−16.

(57) Skoplyak, O.; Barteau, M. A.; Chen, J. G. G. *Surf. Sci.* **2008**, *602*, 3578−3587.

(58) Williams, R. M.; Pang, S. H.; Medlin, J. W. *Surf. Sci.* **2014**, *619*, 114−118.

(59) Henderson, M. A. *Surf. Sci.* **1996**, *355*, 151−166.

(60) Kim, K. S.; Barteau, M. A. *J. Mol. Catal.* **1990**, *63*, 103−117.

(61) Farfan-Arribas, E.; Madix, R. J. *J. Phys. Chem. B* **2002**, *106*, 10680−10692.

(62) Li, M.; Hebenstreit, W.; Diebold, U.; Tyryshkin, A. M.; Bowman, M. K.; Dunham, G. G.; Henderson, M. A. *J. Phys. Chem. B* **2000**, *104*, 4944−4950.

(63) Feng, T.; Vohs, J. M. *J. Phys. Chem. B* **2005**, *109*, 2120−2127.

(64) Lee, S.; Zajac, G. W.; Goodman, D. W. *Top. Catal.* **2006**, *38*, 127−132.

(65) Bu, Y.; Breslin, J.; Lin, M. C. *J. Phys. Chem. B* **1997**, *101*, 1872−1877.

(66) Jeroro, E.; Vohs, J. M. *J. Phys. Chem. C* **2009**, *113*, 1486−1494.

(67) Madhavaram, H.; Idriss, H. *J. Catal.* **2004**, *224*, 358−369.

(68) Zhao, H. B.; Kim, J.; Koel, B. E. *Surf. Sci.* **2003**, *538*, 147−159.

(69) Park, J. B.; Graciani, J.; Evans, J.; Stacchiola, D.; Ma, S. G.; Liu, P.; Nambu, A.; Sanz, J. F.; Hrbek, J.; Rodriguez, J. A. *Proc. Natl. Acad. Sci. U.S.A.* **2009**, *106*, 4975−4980.